Zhang, S., **Adrian, L.**, **Schüürmann, G.** (2018):
Interaction mode and regioselectivity in vitamin B_{12}-dependent dehalogenation of aryl halides by *Dehalococcoides mccartyi* strain CBDB1
Environ. Sci. Technol. **52** (4), 1834 – 1843

Interaction Mode and Regioselectivity in Vitamin B_{12}-Dependent Dehalogenation of Aryl Halides by *Dehalococcoides mccartyi* Strain CBDB1

Shangwei Zhang,[†§] *Lorenz Adrian,*[‡⊥] *and Gerrit Schüürmann*[*†§]

[†]UFZ Department of Ecological Chemistry, Helmholtz Centre for Environmental Research, Permoserstraße 15, 04318 Leipzig, Germany

[‡]UFZ Department of Isotope Biogeochemistry, Helmholtz Centre for Environmental Research, Permoserstraße 15, 04318 Leipzig, Germany

[⊥]Technische Universität Berlin, Chair of Geobiotechnology, Ackerstraße 76, 13355 Berlin, Germany

[§]Technical University Bergakademie Freiberg, Institute for Organic Chemistry, Leipziger Straße 29, 09596 Freiberg, Germany

*Corresponding author:

Gerrit Schüürmann, Tel +49-341-235-1262, Fax +49-341-235-45-1262, Email gerrit.schuurmann@ufz.de.

22 **TOC**

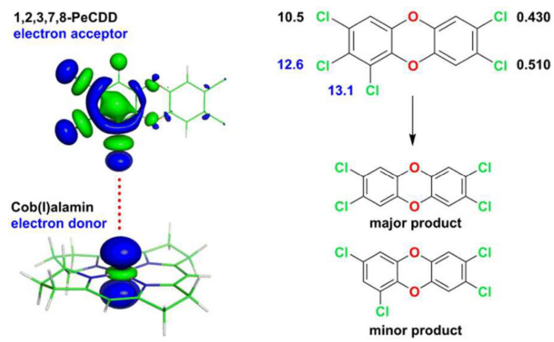
1,2,3,7,8-PeCDD
electron acceptor
Cob(I)alamin
electron donor
10.5
12.6
13.1
0.430
0.510
major product
minor product

23

24

ABSTRACT

The bacterium *Dehalococcoides*, strain CBDB1, transforms aromatic halides through reductive dehalogenation. So far, however, the structures of its vitamin B_{12}-containing dehalogenases are unknown, hampering clarification of the catalytic mechanism and substrate specificity as basis for targeted remediation strategies. This study employs a quantum chemical donor-acceptor approach for the Co(I)-substrate electron transfer. Computational characterization of the substrate electron affinity at carbon-halogen bonds enables discriminating aromatic halides ready for dehalogenation by strain CBDB1 (active substrates) from non-dehalogenated (inactive) counterparts with 92% accuracy, covering 86 of 93 bromobenzenes, chlorobenzenes, chlorophenols, chloroanilines, polychlorinated biphenyls, and dibenzo-*p*-dioxins. Moreover, experimental regioselectivity is predicted with 78% accuracy by a site-specific parameter encoding the overlap potential between the Co(I) HOMO (highest occupied molecular orbital) and the lowest-energy unoccupied sigma-symmetry substrate MO (σ*), and the observed dehalogenation pathways are rationalized with a success rate of 81%. Molecular orbital analysis reveals that the most reactive unoccupied sigma-symmetry orbital of carbon-attached halogen X ($\sigma^*_{C\text{-}X}$) mediates its reductive cleavage. The discussion includes predictions for untested substrates, thus providing opportunities for targeted experimental investigations. Overall, the presently introduced orbital interaction model supports the view that with bacterial strain CBDB1, an inner-sphere electron transfer from the supernucleophile B_{12} Co(I) to the halogen substituent of the aromatic halide is likely to represent the rate-determining step of the reductive dehalogenation.

INTRODUCTION

Aromatic halides such as chlorobenzenes, chlorophenols, polychlorinated biphenyls (PCBs), dibenzo-*p*-dioxins (PCDDs) and dibenzofurans (PCDFs), and polybrominated diphenyl ethers (PBDEs) are ubiquitous xenobiotics due to their intensive use in various applications.[1-5] Various halogenated aromatics such as hexachlorobenzene, PCBs, PCDDs and PCDFs, are considered persistent and have been restricted or banned by the Stockholm Convention.[6]

Detoxification of such halogenated aromatics through reductive dehalogenation by anaerobic microbes may provide a remediation pathway in aquifers and soil. It was shown that aryl halides can be effectively transformed by organohalide-respiring bacteria, which employ these compounds as terminal electron acceptors in anaerobic respiration and derive energy from the electron transfer to these substrates for growth.[7,8] Such organohalide-respiring microbes were found in the *Chloroflexi*, *Firmicutes*, and *Proteobacteria*, and the genes encoding reductive dehalogenase enzymes were identified.[9] Among bacterial isolates, *Dehalococcoides* dehalogenate the broadest variety of aryl halides.[10-12] However, the exact dehalogenation mechanism and its potential substrate specificity have not been clarified, limiting their scope for targeted applications. In this context, major barriers are the low growth yield of strains as compared to the amount of transformed aryl halides, the high oxygen sensitivity of the reductive dehalogenases, and the presence of multiple reductive dehalogenases.[13]

Earlier studies showed that cobalamin is a necessary cofactor for the growth of *Dehalococcoides,* suggesting that the reductive dehalogenation is catalyzed by microbial vitamin B_{12}.[14] In particular, the super-nucleophile cob(I)alamin was recognized as the active species, initiating reductive dehalogenation through electron transfer to the aromatic halide.[15-16] The latter was further demonstrated by recently unraveled crystal structures of two heterologously expressed dehalogenases, NpRdhA from *Nitratireductor pacificus* pht-3B, and PceA from *Sulfurospirillum multivorans*.[17,18] Yet, the structures of the reductive dehalogenases from *Dehalococcoides* are still unknown, leaving also unclarified whether the dehalogenation involves an inner-sphere or outer-sphere electron transfer.

Recently, the three-dimensional structure and EPR measurements of heterologously expressed reductive dehalogenase NpRdhA from *N. pacificus* pht-3B in *Bacillus megaterium* suggested an inner-sphere reaction for cob(I)alamin with 2,6-dihalogenated aromatics.[17] By comparing the ratio of transformation products of trichloroethene catalyzed by cob(I)alamin and well-characterized outer-sphere agents, outer-sphere electron transfer was excluded in B_{12}-dependent reductive dehalogenation.[19] Moreover, Marcus theory analysis showed that enzymatically catalyzed dehalogenation of tri- and tetrachloroethene was not an outer-sphere electron transfer process.[20] These studies imply that the organohalide dehalogenation proceeds through an inner-sphere electron transfer mechanism. Regarding *Dehalococcoides*, however, a respective clarification is still lacking.

Recent studies including computational chemistry suggest a Co⋯Cl interaction during dehalogenation of aryl halides by *Dehalococcoides mccartyi* strain CBDB1.[21,22] Interestingly, the same interaction mode is supported by the structure of the reductive dehalogenase NpRdhA from *N. pacificus* pht-3B.[17] Computational docking with PceA from *S. multivorans* and NpRdhA followed by orbital analyses through density functional theory provided further insight into the Co⋯Cl interaction.[23] However, the sequence similarities between strain CBDB1 and strains pht-3B and *S. multivorans* are only 24% and 29%, respectively (sequence access codes: WP_011308703, CbrA, CBDB1; WP_008597722, NpRdhA, pht-3B; O68252, PceA, *S.*

multivorans).[17] Moreover, these three strains have different substrate ranges and dehalogenation patterns. Strain pht-3B dehalogenates 2,6-halogenated aromatics and abstracts mono-ortho substituted halogens,[17] and strain *S. multivorans* respires halogenated ethenes,[18] whereas strain CBDB1 dehalogenates a wider range of substrates and mainly removes di-ortho substituted halogens.[22] Even with overlapping substrate ranges, different cobalamin-requiring strains may adopt different interaction modes for dehalogenation. For example, cobalamin-employing *Dehalococcoides* and *Dehalobacter* transform chlorobenzenes and chloroanilines with different dehalogenation patterns, suggesting a Co···H interaction as initial dehalogenation step with *Dehalobacter* 14DCB1.[22] Alternatively, a Co···C (*sp*, sp^2) interaction is also viable. For instance, 89% of *cis*-chlorovinylcobalamin was obtained with chloroacetylene as cob(I)alamin substrate,[24,25] suggesting an initial Co···C (*sp*) interaction. In the cobalamin-catalyzed dehalogenation of chloroethenes, mass spectrometry showed that chlorovinylcobalamin and alkylcobalamin were formed, providing the possibility of a Co···C interaction.[26] Moreover, a Co···C (sp^2) would fit to the dehalogenation pathways catalyzed by cobaloxime and cobalamine complexes.[27-30]

In this study, experimental dehalogenation pathways are analyzed with regard to the substrate regioselectivity, covering bromobenzenes, chlorobenzenes, chlorophenols, chloroanilines, polychlorinated biphenyls (PCBs), and dibenzo-*p*-dioxins (PCDDs). To this end, computational chemistry is employed to identify the initial Co(I)···substrate interaction mode through analyses of energetically dominating donor-acceptor molecular orbitals. The results demonstrate that the experimentally observed dehalogenation patterns can be traced back to an inner-sphere Co(I)···halogen donor-acceptor interaction, and provide a theoretical framework for identifying aromatic halides as CBDB1-active substrates (that undergo dehalogenation with this bacterial strain) as well as for predicting the resultant dehalogenation pathways from their site-specific reactivities.

MATERIALS AND METHODS

Data Set. Experimental data for dehalogenation pathways of 93 aryl halides with *Dehalococcoides mccartyi* strain CBDB1 (Tables S1-S3) were taken from literature and cover the following six compound classes: 12 chlorobenzenes (no. 1-12 in Table 1), 5 bromobenzenes (no. 13-17), 19 chlorophenols (no. 18-36), 17 chloroanilines (no. 37-53), 28 polychlorinated biphenyls (PCBs, no. 54-81), and 12 polychlorinated dibenzo-*p*-dioxins (PCDDs, no. 82-93).

Computational Details. Density functional theory (DFT) employing the BP86 functional recommended for cobalamin[31] with basis set Def2-SVP as implemented in Gaussian 09 Revision D.01[32] has been used for the quantum chemical electronic structure calculations including geometry optimization. The starting point of the B_{12} geometry was the X-ray crystal structure of the reductive dehalogenase PceA in *Sulfurospirillum* multivorans.[18] Truncation through replacing the side chains of the corrin ring by H resulted in a 45-atom model of cob(I)alamin (Co(I)Cbl) containing Co^+ and corrin with a deprotonated nitrogen (Figure 1). Decomposition of the molecular orbitals (MOs) into natural bond orbitals (NBOs) and natural atomic orbitals (NAOs) were performed with NBO 6.0.[33]

Donor-Acceptor Reactivity. According to second-order perturbation theory, the interaction of an occupied donor molecular orbital (MO) ϕ_i with an energetically higher unoccupied acceptor MO ϕ_j stabilizes orbital energy ε_i by

$$\varepsilon_i^{(2)} = \frac{\left(H_{ij}-\varepsilon_i\cdot S_{ij}\right)^2}{\varepsilon_i-\varepsilon_j} \approx \frac{(k-\varepsilon_i)^2\cdot S_{ij}^2}{\Delta\varepsilon_{ij}} \qquad (1)$$

per electron, with $\Delta\varepsilon_{ij} = \varepsilon_i - \varepsilon_j$ (that is negative for $\varepsilon_i < \varepsilon_j$).[34] In Eq. 1, the approximation $H_{ij} \approx k \cdot S_{ij}$ with constant k has been introduced to express the rough proportionality between the matrix element $H_{ij} = \langle \phi_i|\hat{H}|\phi_j \rangle$ as integral of the molecular orbitals ϕ_i and ϕ_j with the Hamiltonian $\hat{H}$, and the respective overlap integral $S_{ij} = \langle \phi_i|\phi_j \rangle$. For MOs built from atomic orbitals (AOs) χ_μ according to the linear combination of atomic orbitals to molecular orbitals (LCAO-MO expansion)

$$\phi_i = \sum_\mu c_{\mu i}\, \chi_\mu \qquad (2)$$

with coefficients (weights) $c_{\mu i}$, the MO-based overlap integral S_{ij} can be expressed through AO-based overlap integrals $S_{\mu\nu} = \langle \chi_\mu|\chi_\nu \rangle$ as

$$S_{ij} = \sum_\mu \sum_\nu c_{\mu i} c_{\nu j} S_{\mu\nu} \qquad (3)$$

Taking the square yields

$$S_{ij}^2 = \sum_\mu \sum_\nu c_{\mu i}^2\, c_{\nu j}^2 \cdot S_{\mu\nu}^2 + \text{cross-terms} \qquad (4)$$

as short-hand notation specifying only the terms with squared LCAO-MO coefficients. For ϕ_i representing the HOMO (highest-occupied MO) of Cob(I)alamin as electron donor D, $c_{\mu i}^2$ has a certain but constant value for each AO involved at the Co(I) site. Regarding aromatic halides as substrates, ϕ_j represents the lowest unoccupied MO of interaction-suitable symmetry that acts as electron acceptor A, and so varies for different substrates. Note that because of the symmetry constraint imposed through the interaction mode, ϕ_j is in fact above the LUMO (overall lowest unoccupied MO) for all presently analyzed substrates except higher brominated benzenes (see also Fig. 2 below). For a particular halogen X attached to an aromatic carbon with the X valence *p* orbitals p_x, p_y and p_z as relevant AOs, the squared LCAO-MO coefficient can be written as

$$c_{pX}^2 = c_{p_x X}^2 + c_{p_y X}^2 + c_{p_z X}^2 \qquad (5)$$

Summation over all halogens X attached to aromatic carbons of a given substrate yields

$$c_{p,\,\mathrm{all\,X}}^2 = \sum_{\mathrm{X}} \left(c_{p_x\mathrm{X}}^2 + c_{p_y\mathrm{X}}^2 + c_{p_z\mathrm{X}}^2\right) \qquad (6)$$

Thus the donor-acceptor interaction reactivity ΔE_{DA} defined through

$$\varepsilon_{\mathrm{DA}}^{(2)} \sim \frac{c_{p,\,\mathrm{all\,X}}^2}{\Delta\varepsilon_{\mathrm{DA}}} \equiv \Delta E_{\mathrm{DA}} \qquad (7)$$

may serve as approximate measure for the energy stabilization obtained through electron transfer from Co(I) as electron donor D to the valence-shell *p* AOs that belong to the lowest-energy unoccupied MO of interaction-suitable symmetry and are located at halogen atoms X as electron acceptors A.

Inclusion of the X *s* valence orbitals contributing to the unoccupied substrate ϕ_j of interest yields

$$c_{sp\mathrm{X}}^2 = c_{s\mathrm{X}}^2 + c_{p_x\mathrm{X}}^2 + c_{p_y\mathrm{X}}^2 + c_{p_z\mathrm{X}}^2 \qquad (8)$$

$$c_{sp,\,\mathrm{all\,X}}^2 = \sum_{\mathrm{X}} \left(c_{s\mathrm{X}}^2 + c_{p_x\mathrm{X}}^2 + c_{p_y\mathrm{X}}^2 + c_{p_z\mathrm{X}}^2\right) \qquad (9)$$

$$\varepsilon_{\mathrm{DA}}^{(2)}(sp) \sim \frac{c_{sp,\,\mathrm{all\,X}}^2}{\Delta\varepsilon_{\mathrm{DA}}} \equiv \Delta E_{\mathrm{DA}}(sp) \qquad (10)$$

as correspondingly extended reactivity parameters. The calculations of $c_{p\mathrm{X}}^2$, $c_{sp\mathrm{X}}^2$, ΔE_{DA} and $\Delta E_{\mathrm{DA}}(sp)$ have been performed with Excel employing respective Gaussian outputs.

RESULTS and DISCUSSION

Cob(I)alamin-Substrate Orbital Interaction. Figure 2 shows the highest occupied and lowest unoccupied MOs of Cob(I)alamin (HOMO and LUMO; A left) as well the HOMO and the four lowest unoccupied MOs of pentachlorobenzene (HOMO, LUMO, LUMO+1, LUMO+2, LUMO+3; A right). The HOMO of the supernucleophile cob(I)alamin is essentially the Co 3d_{z2} AO (95.8%; a *d* orbital with lobes along the z axis that belongs to the 3rd electron shell of Co), offering a transfer of one or two electrons to a symmetry-compatible acceptor orbital of the substrate. Here, the interaction geometry with a halogen substituent approaching Co(I) (Figure 2, B) rules out aromatic halide MOs with π symmetry (π* MOs) such as the degenerate LUMO and LUMO+1, both of which would result in a destructive (amplitude-deleting) overlap with the Co(I) 3d_{z2} AO (because two halogen MO lobes of opposite sign approach in parallel one side of the Co(I) 3d_{z2} lobe with just one sign). For the example of PeCB in Figure 2, LUMO+2 is the lowest-energy unoccupied MO with appropriate σ symmetry (σ* MO) allowing for a favourable overlap with Co(I) 3d_{z2}, and thus may act as electron acceptor orbital in an inner-sphere electron transfer reaction.

NBO[32] decomposition of the lowest-energy σ* MOs of the 93 aromatic halide substrates shows that these MOs correspond mainly to the $\sigma^*_{C\text{-}Cl}$ or $\sigma^*_{C\text{-}Br}$ orbitals located at the C–halogen linkages (typically around 60-80%), sometimes with minor contributions from $\sigma^*_{C\text{-}H}$ orbitals (5-13%) at unsubstituted aromatic carbon sites (Table S4). Except for the higher brominated benzenes (Figure S2), these acceptor σ* MOs lie energetically above the substrate LUMO (as π* MO), but represent the lowest-energy substrate orbitals offering a shape suitable for a favourable overlap with the donor Co(I) 3d_{z2} which in turn drives the electron-transfer reaction (Figure 2 and Figures S1-S6).

According to these findings, the Co(I)-catalyzed reductive dehalogenation would proceed through an initial inner-sphere Co^{+1}···X (X = Cl or Br) interaction, transferring one or two electrons from the Co(I) HOMO (3d_{z2}) to the lowest sigma-symmetry vacant MO at C–X ($\sigma^*_{C\text{-}X}$) that weakens the respective $\sigma_{C\text{-}X}$ bond as first step of its cleavage. Further important implications are that in case the CBDB1-catalyzed dehalogenation is governed by this donor-acceptor orbital interaction, the initial site of attack at the substrate would be neither an aromatic carbon (corresponding to the earlier view that Co(I) may attack the olefin carbon followed by β elimination of Cl)[26,35-37] nor an H atom attached to an unsubstituted aromatic carbon. Thus it is of interest whether the experimentally observed dehalogenation patterns would be theoretically expected from the substrate reactivity for the above-described donor-acceptor interaction, which is subject of the next section.

Donor-Acceptor Interaction Reactivity. In the orbital framework of the donor-acceptor interaction, second-order perturbation theory provides an approximate quantification of the energy stabilization in the initial part of the electron-transfer reaction.[34] A further simplification yields the term ΔE_{DA} as rough measure of the donor-acceptor energy stabilization (eq. 7, Section Material and Methods), which in turn is defined as ratio of the sum of (relevant) squared LCAO-MO coefficients at the halogen sites, $c^2_{p,\,\mathrm{all\,X}}$ (the total halogen overlap potential provided through *p* orbitals), over the energy difference of the interacting donor and acceptor orbitals, $\varepsilon_D - \varepsilon_A$. Here, ε_D is the energy of the Co(I) HOMO mainly confined to its $3d_{z2}$ AO at the Co site, whereas ε_A represents the lowest sigma-symmetry vacant (σ*) MO of the substrate with a shape suitable for a favourable (constructive) $3d_{z2}\cdots\sigma^*$ interaction.

In Table 1, the donor-acceptor interaction strength in terms of the ΔE_{DA} parameter is listed for all 93 substrates. For further evaluation, the following three subsets have been formed: Subset I includes all 53 single-ring aromatics (chlorinated benzenes, brominated benzenes, anilines and phenols; no. 1-53 in Table 1), whereas the 28 PCBs and 12 PCDDs form subsets II (no. 54-81) and III (no. 82-93), respectively. Overall, 60 of the 93 aromatic halides are active regarding CBDB1-mediated dehalogenation (see superscript (+) in Table 1), with the remaining 33 compounds being recalcitrant (inactive regarding dehalogenation) when exposed to this bacterial strain (see Tables S1-S3 for experimental information). For subset I, calculated ΔE_{DA}

discriminates experimentally active (ΔE_{DA} < –12.3) from inactive (ΔE_{DA} ≥ –12.3) substrates with only four exceptions (wrongly predicted active: 1,3,5-TrCB, 2,4,6-TrCA; wrongly predicted inactive: 2,4-DCP, 2,5-DCP), which corresponds to a prediction rate of 92%. For subset II, the thresholds ΔE_{DA} ≤ –16.0 and ΔE_{DA} ≥ –15.2 indicate active and inactive PCBs with three wrongly classified congeners (wrongly predicted inactive: 2,4,5-PCB, 2,3,4,6-PCB; wrongly predicted active: 2,4,6-PCB), yielding a prediction rate of 89%. Regarding the PCDD subset III, ΔE_{DA} ≤ –12.2 and ΔE_{DA} ≥ –7.6 discriminate active from inactive substrates. Overall, ΔE_{DA} differentiates between active and inactive aromatic halides regarding CBDB1 with a success rate of 92% (86 of 93 compounds). Similar results are obtained when extending the ΔE_{DA} calculation to include also the valence *s* orbital of the halogen substituents ($\Delta E_{DA}(sp)$, eq. 10; Table S5). Because the misclassified 7 compounds do not differ systematically in their electronic structure from the other substrates, these prediction errors might be due to using a cob(I)almin model without corrinoid side chains, which may be subject to future investigations.

Substrate Reactivity vs. Degree and Type of Halogenation. Inspection of Table 1 reveals further that within a given class of halogenated aromatics, ΔE_{DA} becomes increasingly negative (larger as absolute value) with increasing halogenation of the congener except for some counterexamples. Thus, ΔE_{DA} reflects the experimental finding that with CBDB1, higher halogenated aromatics are generally transformed faster than their lower-halogenated counterparts.[21]

Moreover, the ΔE_{DA} values of the bromobenzenes are below (more stabilizing than) the ones of the chlorobenzenes, indicating the lower electron affinity of the latter. Note in this context that CBDB1 dehalogenates mono-bromobenzene but not mono-chlorobenzene,[38] which is captured by the present ΔE_{DA}-based model, but would fail to be recognized when considering only the topological substitution pattern (e.g.

doubly-flanked halogen) of the CBDB1 substrate. Thus, all bromobenzenes are active substrates of CBDB1 as correctly predicted for the five congeners listed in Table 1 (no. 13-17), yielding lower-brominated benzenes and benzene as metabolites. It suggests further that *Dehalococcoides mccartyi* strain CBDB1 could in principle convert all bromobenzenes to benzene as ultimate metabolite.

Another experimental finding reflected by ΔE_{DA} is the impact of the substitution pattern on the rate of reductive dehalogenation. With 1,2,3-TrCB and 1,2,4-TrCB used together as substrates for CBDB1, 1,2,4-TrCB was not dehalogenated until 1,2,3-TrCB was almost used up.[39] In accord with this result, calculated ΔE_{DA} is larger negative for 1,2,3-TrCB as preferred (and faster degrading) substrate. Moreover, when comparing 2,3-DCA,1,2-DCB, 2,3-DCP and 1,2,3-TrCB, dehalogenation reactivity increases with increasing electron-withdrawing power of the substituents,[21,22] which correlates also with the respective ΔE_{DA} values.

Finally, ΔE_{DA} indicates that the reductive dehalogenation reactivity of two-ring aromatic halides is similar to that of higher halogenated mono-ring derivatives (Figures S7-S8). For example, 2,3-DCDD (dichloro-dibenzo-*p*-dioxin) was transformed by strain CBDB1 while 2,7-DCDD and 2,8-DCDD were not.[40] Indeed, the ΔE_{DA} values of the latter two congeners are similar to that of non-active 2-MCDD, but significantly less negative than that of 2,3-DCDD, indicating 2,3-DCDD is CBDB1-active whereas 2,7-DCDD and 2,8-DCDD are not.

Overlap vs Energy Component of Donor-Acceptor Interaction. The inner-sphere electron-transfer reactivity parameter ΔE_{DA} contains two components (eq. 7, section Materials and Methods) that both affect the strength of the orbital interaction when the electron donor and acceptor approach each other. The numerator ($c^2_{p,\,\mathrm{all\,X}}$; eq. 6, section Material and Methods) encodes the potential for spatial overlap between the valence-shell *p* orbitals of the lowest substrate σ* MO and a donor orbital with suitable shape (symmetry) at all possible halogen sites. The denominator, $\varepsilon_D - \varepsilon_A$, scales the energy stabilization inversely to the difference of the initial (unperturbed) energies of the donor and acceptor orbital.

Interestingly, subset I (53 mono-ring substrates) shows a surprisingly high correlation between these two components ($r^2 = 0.88$; $\Delta E_{DA} = a \cdot c^2_{p,\,\mathrm{all\,X}} + b$ with slope a = 0.096, intercept b = –5.6, Figure 3), and for subsets II (28 PCBs) and III (12 PCDDs) the respective correlations are still significant if in each of the latter subsets two outliers are excluded (r^2 = 0.80 vs 0.88, slope = 0.066 vs 0.069, intercept = –4.4 vs –4.3, Figures S9-S10). These findings indicate that regarding the reductive dehalogenation of the aromatic halides initiated by electron transfer from Co(I) to halogen substituents, the substrate reactivity appears to depend in a similar manner on the overlap potential (summed over all potential halogen sites) and the difference in Co(I) HOMO (= $3d_{z2}$) and lowest-energy substrate σ* MO energies. Thus, both the halogen overlap potential ($c^2_{p,\,\mathrm{all\,X}}$) and the donor-acceptor orbital energy difference ($\varepsilon_D - \varepsilon_A$) alone discriminate also reasonably well active from inactive aromatic halides (90% vs 86%, Tables S6-S7). Future investigations may show whether this holds also for polyhalogenated aromatics containing more than one halogen atom type.

Regioselectivity and Dehalogenation Pathway. The donor-acceptor reactivity parameter ΔE_{DA} encodes the overall substrate potential for a reaction-inducing overlap through its lowest σ* MO at any possible halogen site. As such, ΔE_{DA} cannot discriminate between different site-specific reactivities of a given substrate. The latter, however, can be achieved through evaluating $c^2_{p\mathrm{X}}$ (eq. 5, section Materials and Methods) that quantifies the overlap potential of the lowest σ* MO through its three valence-shell p orbitals (p_x, p_y, p_z) at a particular halogen site X (X = Cl or Br).

In Tables 2 and S8-S9, the respective $c_{p\mathrm{X}}^2$ values are listed for all halogen sites of all 59 substrates that should be amenable to dehalogenation according to their electron-acceptor reactivity ΔE_{DA}. Taking 1,2,4-TrCB as example, the largest $c_{p\mathrm{X}}^2$ value is obtained for Cl attached to aromatic carbon C_2, (15.6 vs 11.3 at C_1 vs 7.22 at C_4), and indeed 1,4-DCB is obtained as major metabolite with a ratio 7:3 as compared to the second metabolite 1,3-DCB.[41] For 1,2,3,7,8-PeCDD (last line in Table 2), $c_{p\mathrm{X}}^2$ indicates that Cl at C_1 and C_2 are preferred for CBDB1-catalyzed reductive dehalogenation, which is confirmed by the experimental finding of 2,3,7,8-TeCDD and 1,3,7,8-TeCDD as metabolites.[40]

Overall, the site-specific halogen overlap potential ($c_{p\mathrm{X}}^2$) identifies the most reactive halogen substituent with a success rate of 78% (38 of 49 CBDB1-active substrates with opportunity for regioselective dehalogenation), and is compatible with the experimentally observed dehalogenation pathways with a success rate of 81% (48 out of 59 active substrates). Taking 1,2,4-TrBB as further example, the bromine substituents at C_1, C_2 and C_4 yield $c_{p\mathrm{X}}^2$ values of 14.5, 20.4, and 7.76, respectively (Table 2), indicating Br at C_2 as most reactive for CBDB1-mediated dehalogenation. It follows that in this case, calculated $c_{p\mathrm{X}}^2$ predicts 1,4-DBB as major metabolite, which agrees with experimental observation.[38] Deviations between $c_{p\mathrm{X}}^2$-based regioselectivity and experiment, however, are obtained for 11 substrates (1,2,3,5-TeCB, 2,3,6-TrCP, 2,4,5-TrCP, 3,4-DCA, 2,3,5-TrCA, 2,3,4,6-TeCA, 2,3,4-2,3-PCB, 2,3,4,2',4'-PCB, 2,3,4,2',5'-PCB, 2,3,4,2',3',4'-PCB and 1,2,4-TrCDD). Similar results are obtained when including the halogen valence *s* orbital in the halogen overlap potential (parameter $c_{sp\mathrm{X}}^2$, eq. 8; Tables S10-S12). Although there is certainly room for improvement, these findings demonstrate the power of our simplified orbital interaction approach to identify primary sites of CBDB1-mediated Co(I) attack as first step in the reductive dehalogenation of aromatic halides.

Experimentally Untested Substrates. 2,3,6-TrCA and 2,3,4,5-TeCA are two commercially unavailable chloroanilines that should be substrates for strain CBDB1 according to our ΔE_{DA} reactivity parameter (Table S13). The expected metabolites are 2,5-DCA from 2,3,6-TrCA as well as 2,4,5-TrCA (major) and 2,3,5-TrCA from 2,3,4,5-TeCA (Figure 4A, Tables S14-S15), suggesting similar dehalogenation pathways as observed for their chlorophenol counterparts.[10]

Seven untested bromobenzenes are also predicted through their ΔE_{DA} values to be CBDB1 substrates (Table S13). Here, the site-specific parameter $c_{p\mathrm{X}}^2$ indicates the following expected dehalogenation patterns (Figure 4B and Tables S14-S15): 1,2,3-TrBB and 1,3,5-TrBB are transformed to 1,3-DBB, 1,2,3,4-TeBB and 1,2,4,5-TeBB yield 1,2,4-TrBB, PeBB is dehalogenated to 1,2,3,5-TeBB and 1,2,4,5-TeBB, and HBB is converted to PeCB. Except for 1,3,5-TrBB, these predicted pathways of bromobenzenes are similar to the experimentally known dehalogenation pathways of chlorobenzenes with strain CBDB1 (Table S1). However, site-specific $c_{p\mathrm{X}}^2$ would not predict 1,3,5-TrBB as primary metabolite of 1,2,3,5-TeBB, thus contrasting with the observed CBDB1 metabolite 1,3,5-TrCB of 1,2,3,5-TeCB.[41]

According to the sequenced genome, *Dehalococcoides mccartyi* strain CBDB1 harbors 32 reductive dehalogenase homologous genes,[42] which indicates its great potential for detoxifying organohalides in environmental matrices. So far, however, no dehalogenase structure of this species has been determined, with the low growth yield of strain CBDB1 and obstructions with the heterologous expression of these complex metalloproteins representing major technical barriers. Nevertheless, computational chemistry may provide insight into the mechanism underlying the CBDB1-mediated reductive dehalogenation. To this end, the presently introduced donor-acceptor orbital interaction perspective supports the view that with these bacteria, inner-sphere electron transfer from B_{12} Co(I) to the halogen substituent represents the rate-determining step. A further way forward could be a quantum chemical analysis of Co(I)-catalyzed transition states of the dehalogenation reaction, following an approach undertaken for the cytochrome P450 catalysis without[43-45] or with[46] inclusion of coupling quantum chemistry with molecular mechanics. Finally, including selected side-chains for an accordingly augmented model of cob(I)alamin may provide insight whether and how corrinoid side-chains could affect the redox activity, and how the latter might also be triggered by the cob(I)alamin base-off state as opposed to a possibly preceding corrinoid base-on state.

ASSOCIATED CONTENT

Supporting information

The Supporting Information is available free of charge on ACS Publications website at DOI...

Notes

The authors declare no competing financial interest.

REFERENCES

(1) Häggblom, M. M.; Bossert, I. D. Halogenated organic compounds - A global perspective. In: Häggblom, M. M.; Bossert, I. D. (eds.) *Dehalogenation*, Kluwer, **2004**, pp 3-29.

(2) Wania, F.; Mackay, D. Tracking the Distribution of Persistent Organic Pollutants. *Environ. Sci. Technol*. **1996**, *30* (9), 390A-396A.

(3) Jones, K. C.; de Voogt, P. Persistent organic pollutants (POPs): state of the science. *Environ. Pollut*. **1999**, *100* (1-3), 209-221.

(4) Xu, W.; Wang, X.; Cai, Z. Analytical chemistry of the persistent organic pollutants identified in the Stockholm convention: A review. *Anal. Chim. Acta* **2013**, *790*, 1-13.

(5) Lundin, J. I.; Ylitalo, G. M.; Booth, R. K.; Anulacion, B.; Hempelmann, J. A.; Parsons, K. M.; Giles, D. A.; Seely, E. A.; Hanson, M. B.; Emmons, C. K.; Wasser, S. K. Modulation in Persistent Organic Pollutant Concentration and Profile by Prey Availability and Reproductive Status in Southern Resident Killer Whale Scat Samples. *Environ. Sci. Technol*. **2016**, *50* (12), 6506-6516.

(6) Lallas, P.L. The Stockholm Convention on Persistent Organic Pollutants. *Am. J. Internat. Law* **2001**, *95* (3), 692-708.

(7) Villemur, R. The pentachlorophenol-dehalogenating *Desulfitobacterium hafniense* strain PCP-1. *Philos. Trans. R. Soc. London, B* **2013**, *368* (1616), 20120319.

(8) Leys, D.; Adrian, L.; Smidt, H. Organohalide respiration: microbes breathing chlorinated molecules. *Philos. Trans. R. Soc. London, B* **2013**, *368* (1616), 20120316.

(9) Hug, L. A.; Maphosa, F.; Leys, D.; Löffler, F. E.; Smidt, H.; Edwards, E. A.; Adrian, L. Overview of organohalide-respiring bacteria and a proposal for a classification system for reductive dehalogenases. *Philos. Trans. R. Soc. London, B* **2013**, *368* (1616), 20120322.

(10) Löffler, F. E.; Ritalahti, K. M.; Zinder, S. H. *Dehalococcoides* and reductive dechlorination of chlorinated solvents. In: Stroo, H. F.; Leeson, A.; Ward, C. H. (eds.) *Bioaugmentation for groundwater remediation*, Springer: **2013**; pp 39-88.

(11) Hendrickson, E. R.; Payne, J. A.; Young, R. M.; Starr, M. G.; Perry, M. P.; Fahnestock, S.; Ellis, D. E.; Ebersole, R. C. Molecular analysis of *Dehalococcoides* 16S ribosomal DNA from chloroethene-contaminated sites throughout North America and Europe. *Appl. Environ. Microbiol*. **2002**, *68* (2), 485-495.

(12) Müller, J. A.; Rosner, B. M.; Von Abendroth, G.; Meshulam-Simon, G.; McCarty, P. L.; Spormann, A. M. Molecular identification of the catabolic vinyl chloride reductase from *Dehalococcoides* sp. strain VS and its environmental distribution. *Appl. Environ. Microbiol*. **2004**, *70* (8), 4880-4888.

(13) Jugder, B.-E.; Ertan, H.; Lee, M.; Manefield, M.; Marquis, C. P. Reductive dehalogenases come of age in biological destruction of organohalides. *Trends Biotechnol*. **2015**, *33* (10), 595-610.

(14) Schipp, C. J.; Marco-Urrea, E.; Kublik, A.; Seifert, J.; Adrian, L. Organic cofactors in the metabolism of *Dehalococcoides mccartyi* strains. *Philos. Trans. R. Soc. London, B* **2013**, *368* (1616), 20120321.

(15) Parthasarathy, A.; Stich, T. A.; Lohner, S. T.; Lesnefsky, A.; Britt, R. D.; Spormann, A. M. Biochemical and EPR-spectroscopic investigation into heterologously expressed vinyl chloride reductive dehalogenase (VcrA) from *Dehalococcoides mccartyi* strain VS. *J. Am. Chem. Soc*. **2015**, *137* (10), 3525-3532.

(16) Neumann, A.; Wohlfarth, G.; Diekert, G. Purification and characterization of tetrachloroethene reductive dehalogenase from *Dehalospirillum multivorans*. *J. Biol. Chem*. **1996**, *271* (28), 16515-16519.

(17) Payne, K. A.; Quezada, C. P.; Fisher, K.; Dunstan, M. S.; Collins, F. A.; Sjuts, H.; Levy, C.; Hay, S.; Rigby, S. E.; Leys, D. Reductive dehalogenase structure suggests a mechanism for B12-dependent dehalogenation. *Nature* **2015**, *517* (7535), 513-516.

(18) Bommer, M.; Kunze, C.; Fesseler, J.; Schubert, T.; Diekert, G.; Dobbek, H. Structural basis for organohalide respiration. *Science* **2014**, *346* (6208), 455-458.

(19) Follett, A. D.; McNeill, K. Reduction of trichloroethylene by outer-sphere electron-transfer agents. *J. Am. Chem. Soc*. **2005**, *127* (3), 844-845.

(20) Costentin, C.; Robert, M.; Savéant, J.-M. Does catalysis of reductive dechlorination of tetra- and trichloroethylenes by vitamin B_{12} and corrinoid-based dehalogenases follow an electron transfer mechanism? *J. Am. Chem. Soc*. **2005**, *127* (35), 12154-12155.

(21) Cooper, M.; Wagner, A.; Wondrousch, D.; Sonntag, F.; Sonnabend, A.; Brehm, M.; Schüürmann, G.; Adrian, L. Anaerobic microbial transformation of halogenated aromatics and fate prediction using electron density modeling. *Environ. Sci. Technol*. **2015**, *49* (10), 6018-6028.

(22) Zhang, S.; Wondrousch, D.; Cooper, M.; Zinder, S. H.; Schüürmann, G.; Adrian, L. Anaerobic Dehalogenation of Chloroanilines by *Dehalococcoides mccartyi* Strain CBDB1 and *Dehalobacter* Strain 14DCB1 via Different Pathways as Related to Molecular Electronic Structure. *Environ. Sci. Technol*. **2017**, *51* (7), 3714–3724.

(23) Johannissen, L. O.; Leys, D.; Hay, S. A common mechanism for coenzyme cobalamin-dependent reductive dehalogenases. *Phys. Chem. Chem. Phys*. **2017**, *19* (8), 6090-6094.

(24) McCauley, K. M.; Wilson, S. R.; van der Donk, W. A. Characterization of chlorovinylcobalamin, a putative intermediate in reductive degradation of chlorinated ethylenes. *J. Am. Chem. Soc*. **2003**, *125* (15), 4410-4411.

(25) McCauley, K. M.; Pratt, D. A.; Wilson, S. R.; Shey, J.; Burkey, T. J.; van der Donk, W. A. Properties and reactivity of chlorovinylcobalamin and vinylcobalamin and their implications for vitamin B_{12}-catalyzed reductive dechlorination of chlorinated alkenes. *J. Am. Chem. Soc*. **2005**, *127* (4), 1126-1136.

(26) Lesage, S.; Brown, S.; Millar, K. A different mechanism for the reductive dechlorination of chlorinated ethenes: Kinetic and spectroscopic evidence. *Environ. Sci. Technol*. **1998**, *32* (15), 2264-2272.

(27) Bühl, M.; Golubnychiy, V. On the intermediacy of chlorinated alkylcobalt complexes in the reductive dehalogenation of chloroalkenes. A first-principles molecular dynamics study. *Organometallics* **2007**, *26* (25), 6213-6218.

(28) Follett, A. D.; McNeill, K. Evidence for the Formation of a cis-Dichlorovinyl Anion upon Reduction of cis-1, 2-Dichlorovinyl (pyridine) cobaloxime. *Inorg. Chem*. **2006**, *45* (6), 2727-2732.

(29) Follett, A. D.; McNabb, K. A.; Peterson, A. A.; Scanlon, J. D.; Cramer, C. J.; McNeill, K. Characterization of Co-C bonding in dichlorovinylcobaloxime complexes. *Inorg. Chem*. **2007**, *46* (5), 1645-1654.

(30) Kliegman, S.; McNeill, K. Dechlorination of chloroethylenes by cob (I) alamin and cobalamin model complexes. *Dalton Trans*. **2008** (32), 4191-4201.

(31) Kornobis, K.; Kumar, N.; Wong, B. M.; Lodowski, P.; Jaworska, M.; Andruniów, T.; Ruud, K.; Kozlowski, P. M. Electronically excited states of vitamin B_{12}: benchmark calculations including time-dependent density functional theory and correlated ab initio methods. *J. Phys. Chem. A* **2011**, *115* (7), 1280-1292.

(32) Frisch, M. J.; Trucks, G. W.; Schlegel, H. B.; Scuseria, G. E.; Robb, M. A.; Cheeseman, J. R.; Scalmani, G.; Barone, V.; Mennucci, B.; Petersson, G. A.; Nakatsuji, H.; Caricato, M.; Li, X.; Hratchian, H. P.; Izmaylov, A. F.; Bloino, J.; Zheng, G.; Sonnenberg, J. L.; Hada, M.; Ehara, M.; Toyota, K.; Fukuda, R.; Hasegawa, J.; Ishida, M.; Nakajima, T.; Honda, Y.; Kitao, O.; Nakai, H.; Vreven, T.; Montgomery Jr., J. A.; Peralta, J. E.; Ogliaro, F.; Bearpark, M. J.; Heyd, J.; Brothers, E. N.; Kudin, K. N.; Staroverov, V. N.; Kobayashi, R.; Normand, J.; Raghavachari, K.; Rendell, A. P.; Burant, J. C.; Iyengar, S. S.; Tomasi, J.; Cossi, M.; Rega, N.; Millam, N. J.; Klene, M.; Knox, J. E.; Cross, J. B.; Bakken, V.; Adamo, C.; Jaramillo, J.; Gomperts, R.; Stratmann, R. E.; Yazyev, O.; Austin, A. J.; Cammi, R.; Pomelli, C.; Ochterski, J. W.; Martin, R. L.; Morokuma, K.; Zakrzewski, V. G.; Voth, G. A.; Salvador, P.; Dannenberg, J. J.; Dapprich, S.; Daniels, A. D.; Farkas, Ö.; Foresman, J. B.; Ortiz, J. V.; Cioslowski, J.; Fox, D. J. *Gaussian 09, Revision D.01*, Gaussian, Inc.: Wallingford, CT, USA, **2013**.

(33) Glendening, E. D.; Badenhoop, J, K.; Reed, A. E.; Carpenter, J. E.; Bohmann, J. A.; Morales, C. M.; Landis, C. R.; Weinhold, F. *NBO 6.0*, Theoretical Chemistry Institute, University of Wisconsin, Madison, **2013**.

(34) Albright, T. A.; Burdett, J. K.; Whangbo, M.-H. *Orbital Interactions in Chemistry*. 2nd Edition. Wiley **2013**, pp 32-46.

(35) Banerjee, R.; Ragsdale, S. W. The many faces of Vitamin B_{12}: catalysis by cobalamin-dependent enzymes. *Annu. Rev. Biochem*. **2003**, *72* (1), 209-247.

(36) Holliger, C.; Wohlfarth, G.; Diekert, G. Reductive dechlorination in the energy metabolism of anaerobic bacteria. *FEMS Microbiol. Rev*. **1999**, *22* (5), 383-398.

(37) Wohlfarth, G.; Diekert, G. Anaerobic dehalogenases. *Curr. Opin. Biotechnol*. **1997**, *8* (3), 290-295.

(38) Wagner, A.; Cooper, M.; Ferdi, S.; Seifert, J.; Adrian, L. Growth of *Dehalococcoides mccartyi* strain CBDB1 by reductive dehalogenation of brominated benzenes to benzene. *Environ. Sci. Technol*. **2012**, *46* (16), 8960-8968.

(39) Adrian, L.; Manz, W.; Szewzyk, U.; Görisch, H. Physiological characterization of a bacterial consortium reductively dechlorinating 1, 2, 3-and 1, 2, 4-trichlorobenzene. *Appl. Environ. Microbiol*. **1998**, *64* (2), 496-503.

(40) Bunge, M.; Adrian, L.; Kraus, A.; Opel, M.; Lorenz, W. G.; Andreesen, J. R.; Görisch, H.; Lechner, U. Reductive dehalogenation of chlorinated dioxins by an anaerobic bacterium. *Nature* **2003**, *421* (6921), 357-360.

(41) Adrian, L.; Szewzyk, U.; Wecke, J.; Görisch, H. Bacterial dehalorespiration with chlorinated benzenes. *Nature* **2000**, *408* (6812), 580-583.

(42) Wagner, A.; Segler, L.; Kleinsteuber, S.; Sawers, G.; Smidt, H.; Lechner, U. Regulation of reductive dehalogenase gene transcription in *Dehalococcoides mccartyi*. *Philos. Trans. R. Soc. London, B* **2013**, *368* (1616), 20120317.

(43) Ji, L.; Schüürmann, G. Computational evidence for α-nitrosamino radical as initial metabolite for both the P450 dealkylationand denitrosation of carcinogenic nitrosamines. *J. Phys. Chem. B* **2012**,*116* (2), 903−912.

(44) Ji, L.; Schüürmann, G. Model and Mechanism: N-Hydroxylation of Primary Aromatic Amines by Cytochrome P450. *Angew. Chem. Int. Ed*. **2013**, *52* (2), 744−748. *Angew. Chem*. **2013**, *125* (2), 772−776.

(45) Ji, L.; Schüürmann, G. Computational biotransformation profile of paracetamol catalyzed by cytochrome P450. *Chem. Res. Toxicol*. **2015**, *28* (4), 585−596.

(46) Senn, H. M.; Thiel, W. QM/MM Methods for Biomolecular Systems. *Angew. Chem. Int. Ed*. **2009**, *48* (7), 1198-1229; *Angew. Chem*. **2009**, *121* (7), 1220-1254.

Tables

Table 1. Substrate reactivity in terms of the donor-acceptor interaction parameter ΔE_{DA} [%/eV] characterizing the ease of inner-sphere electron transfer from cob(I)alamin to aromatic halides[a]

No.	Subset	Substrate[b]	ΔE_{DA}	No.	Subset	Substrate[b]	ΔE_{DA}	No.	Subset	Substrate[b]	ΔE_{DA}	No.	Subset	Substrate[b]	ΔE_{DA}
1	I	MCB	–7.85	*26*	I	3,5-DCP	–12.3	*51*	I	2,3,4,6-TeCA$^{(+)}$	–22.4	*76*	II	2,3,4,2',3'-PCB$^{(+)}$	–20.5
2	I	1,2-DCB$^{(+)}$	–13.6	*27*	I	2,3,4-TrCP$^{(+)}$	–22.4	*52*	I	2,3,5,6-TeCA$^{(+)}$	–17.6	*77*	II	2,3,4,2',4'-PCB$^{(+)}$	–20.5
3	I	1,3-DCB	–12.0	*28*	I	2,3,5-TrCP$^{(+)}$	–18.6	*53*	I	PeCA$^{(+)}$	–32.4	*78*	II	2,3,4,2',5'-PCB$^{(+)}$	–20.5
4	I	1,4-DCB	–8.94	*29*	I	2,3,6-TrCP$^{(+)}$	–16.7	*54*	II	2,4-PCB	–11.6	*79*	II	2,3,4,2',3',4'-PCB$^{(+)}$	–22.2
5	I	1,2,3-TrCB$^{(+)}$	–20.2	*30*	I	2,4,5-TrCP$^{(+)}$	–15.7	*55*	II	2,5-PCB	–8.60	*80*	II	2,3,4,2',4',5'-PCB$^{(+)}$	–21.1
6	I	1,2,4-TrCB$^{(+)}$	–16.1	*31*	I	2,4,6-TrCP$^{(+)}$	–18.8	*56*	II	3,5-PCB	–12.2	*81*	II	2,4,5,2',4',5'-PCB$^{(+)}$	–17.2
7	I	1,3,5-TrCB	–17.6	*32*	I	3,4,5-TrCP$^{(+)}$	–20.0	*57*	II	2,3,4-PCB$^{(+)}$	–18.3	*82*	III	2-MCDD	–7.52
8	I	1,2,3,4-TeCB$^{(+)}$	–26.3	*33*	I	2,3,4,5-TeCP$^{(+)}$	–29.8	*58*	II	2,3,5-PCB	–15.2	*83*	III	1,3-DCDD$^{(+)}$	–12.3
9	I	1,2,3,5-TeCB$^{(+)}$	–25.1	*34*	I	2,3,4,6-TeCP$^{(+)}$	–28.0	*59*	II	2,3,6-PCB	–15.2	*84*	III	2,3-DCDD$^{(+)}$	–13.8
10	I	1,2,4,5-TeCB$^{(+)}$	–20.9	*35*	I	2,3,5,6-TeCP$^{(+)}$	–23.6	*60*	II	2,4,5-PCB$^{(+)}$	–11.8	*85*	III	2,7-DCDD	–7.31
11	I	PeCB$^{(+)}$	–35.6	*36*	I	PeCP$^{(+)}$	–38.7	*61*	II	2,4,6-PCB	–16.5	*86*	III	2,8-DCDD	–7.65
12	I	HCB$^{(+)}$	–53.8	*37*	I	2-MCA	–8.32	*62*	II	3,4,5-PCB$^{(+)}$	–18.5	*87*	III	1,2,3-TrCDD$^{(+)}$	–21.1
13	I	MBB$^{(+)}$	–15.7	*38*	I	3-MCA	–7.61	*63*	II	2,3,4,5-PCB$^{(+)}$	–18.7	*88*	III	1,2,4-TrCDD$^{(+)}$	–17.0
14	I	1,2-DBB$^{(+)}$	–27.6	*39*	I	4-MCA	–6.61	*64*	II	2,3,4,6-PCB$^{(+)}$	–9.77	*89*	III	2,3,7-TrCDD$^{(+)}$	–14.1
15	I	1,3-DBB$^{(+)}$	–24.2	*40*	I	2,3-DCA$^{(+)}$	–13.5	*65*	II	2,3,2',3'-PCB	–15.1	*90*	III	1,2,3,4-TeCDD$^{(+)}$	–19.4
16	I	1,4-DBB$^{(+)}$	–17.6	*41*	I	2,4-DCA	–11.4	*66*	II	2,3,2',4'-PCB	–14.1	*91*	III	1,3,7,8-TeCDD$^{(+)}$	–20.0
17	I	1,2,4-TrBB$^{(+)}$	–34.9	*42*	I	2,5-DCA	–8.94	*67*	II	2,3,2',5'-PCB	–14.0	*92*	III	2,3,7,8-TeCDD$^{(+)}$	–14.6
18	I	2-MCP	–7.66	*43*	I	2,6-DCA	–12.2	*68*	II	2,4,2',4'-PCB	–12.6	*93*	III	1,2,3,7,8-PeCDD$^{(+)}$	–22.9
19	I	3-MCP	–7.95	*44*	I	3,4-DCA$^{(+)}$	–12.3	*69*	II	2,4,2',5'-PCB	–12.2				
20	I	4-MCP	–7.01	*45*	I	3,5-DCA	–11.3	*70*	II	2,5,2',5'-PCB	–10.0				
21	I	2,3-DCP$^{(+)}$	–15.9	*46*	I	2,3,4-TrCA$^{(+)}$	–18.2	*71*	II	2,3,5,6-PCB	–20.0				
22	I	2,4-DCP$^{(+)}$	–11.3	*47*	I	2,3,5-TrCA$^{(+)}$	–15.6	*72*	II	2,3,4,5,6-PCB$^{(+)}$	–33.3				
23	I	2,5-DCP$^{(+)}$	–9.15	*48*	I	2,4,5-TrCA$^{(+)}$	–14.6	*73*	II	2,4,5,2',3'-PCB$^{(+)}$	–16.3				
24	I	2,6-DCP$^{(+)}$	–13.5	*49*	I	2,4,6-TrCA	–16.4	*74*	II	2,4,5,2',4'-PCB$^{(+)}$	–16.1				
25	I	3,4-DCP$^{(+)}$	–13.2	*50*	I	3,4,5-TrCA$^{(+)}$	–18.0	*75*	II	2,4,5,2',5'-PCB$^{(+)}$	–16.1				

[a] The 93 aromatic halides comprise 53 single-ring aromatics (subset I) with 12 chlorobenzenes (no. 1-12), 5 bromobenzenes (no. 13-17), 19 chlorophenols (no. 18-36), and 17 chloroanilines (no. 37-53), 28 polychlorinated biphenyls (subset II, no. 54-81), and 12 polychlorinated dibenzo-*p*-dioxins (subset III, no. 82-93).The

substrate reactivity parameter ΔE_{DA} encodes the overlap potential with valence-shell *p* orbitals of all halogen substituents as related to the energy difference between the cob(I)amin HOMO and the lowest σ* substrate MO of overlap-suitable shape (eq. 7, section Material and Methods); increasingly negative ΔE_{DA} indicates an increasing electron-acceptor strength of the substrate. Substrate notation: CB = chlorobenzene, MCB = monochlorobenzene, DCB = dichlorobenzene, TrCB = trichlorobenzene, TeCB = tetrachlorobenzene, PeCB = pentachlorobenzene, HCB = hexachlorobenzene; BB = bromobenzene; CP = chlorophenol; CA = chloroaniline; PCB = polychlorinated biphenyl; DD = dibenzo-*p*-dioxin.

[b] The 60 active substrates undergoing CBDB1-mediated dehalogenation are indicated by the superscript (+). The 7 substrates predicted wrongly as active (no. 7, 49, 61) or wrongly as inactive (no. 22, 23, 60, 64) are underlined. For more detailed experimental information, see Tables S1-S3.

Table 2. Regiospecific halogen overlap potential $c_{p\mathrm{X}}^2$ of CBDB1 substrates as electron acceptor through the valence-shell *p* orbitals of their lowest-energy σ* MO[a]

Aromatic halide	Subset	Halogen substituent position at aromatic ring							
		C_1	C_2	C_3	C_4	C_5	C_6	C_7	C_8
Chlorobenzenes									
1,2,3-TrCB	I	12.3	14.6	12.3					
1,2,4-TrCB	I	11.3	15.6		7.22				
1,2,3,4-TeCB	I	7.89	12.9	12.9	7.89				
1,2,3,5-TeCB	I	11.8	10.7	11.8		5.95			
1,2,4,5-TeCB	I	9.14	9.13	9.13	9.14				
PeCB	I	7.17	8.88	11.8	8.88	7.17			
Bromobenzenes									
1,2-DBB	I	21.4	21.4						
1,3-DBB	I	19.9		19.9					
1,4-DBB	I	16.8			16.8				
1,2,4-TrBB	I	14.5	20.4		7.76				
Chlorophenols									
2,3-DCP	I		20.4	15.0					
3,4-DCP	I			17.1	16.7				
2,3,4-TrCP	I		16.1	14.2	9.51				
2,3,5-TrCP	I		16.0	15.2		4.68			
2,3,6-TrCP	I		12.8	8.23			13.3		
2,4,5-TrCP	I		6.23		14.7	13.1			
2,4,6-TrCP	I		17.1		9.19		9.43		
3,4,5-TrCP	I			11.9	14.0	13.6			
2,3,4,5-TeCP	I		11.5	13.6	12.4	6.18			
2,3,4,6-TeCP	I		15.5	11.0	9.35		5.0		
2,3,5,6-TeCP	I		7.04	6.59	10.5	13.8			
PeCP	I		6.26	7.32	10.1	9.95	10.5		
Chloroanilines									
2,3-DCA	I		18.7	16.3					
3,4-DCA	I			17.5	16.0				
2,3,4-TrCA	I		13.7	14.3	10.4				
2,4,5-TrCA	I		9.25		14.1	10.6			
3,4,5-TrCA	I			12.7	14.0	12.7			
2,3,5,6-TeCA	I		8.76	7.67		7.67	8.76		
Polychlorinated biphenyls									
2,3,4-PCB	II		11.1	14.4	11.4				
3,4,5-PCB	II			11.9	13.8	11.9			
2,3,4,5-PCB	II		5.64	9.02	9.33	5.97			
2,3,4,5,6-PCB	II		6.90	9.24	12.2	9.24	6.90		
Polychlorinated dibenzodioxins									
1,2,3-TrCDD	III	13.4	13.4	11.2					
1,2,4-TrCDD	III	11.5	12.8		8.32				
2,3,7-TrCDD	III		15.7	15.8				0.510	
1,2,3,4-TeCDD	III	8.66	11.5	11.5	8.66				
1,3,7,8-TeCDD	III	9.28		6.58				6.35	6.29
2,3,7,8-TeCDD	III		7.22	7.22				7.22	7.22
1,2,3,7,8-PeCDD	III	13.1	12.6	10.5				0.430	0.510

[a] Subsets I, II and III comprise single-ring aromatics, polychlorinated biphenyls, and polychlorinated dibenzo-*p*-dioxins, respectively.The site-specific parameter $c_{p\mathrm{X}}^2$ (eq. 5, section Materials and Methods)

represents the overlap potential of a particular halogen substituent through its three valence-shell *p* orbitals of the lowest σ* MO of the electron-accepting substrate.

Figures

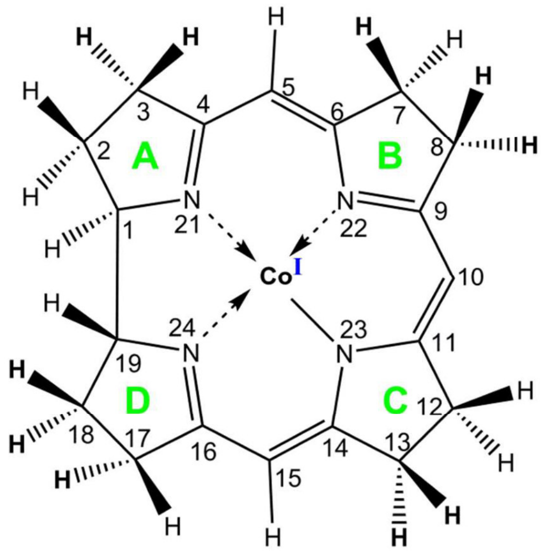

Figure 1. The structure of truncated Cob(I)alamin consisting of Co^+ coordinated by corrin with a deprotonated nitrogen ($C_{19}H_{21}N_4^-$).

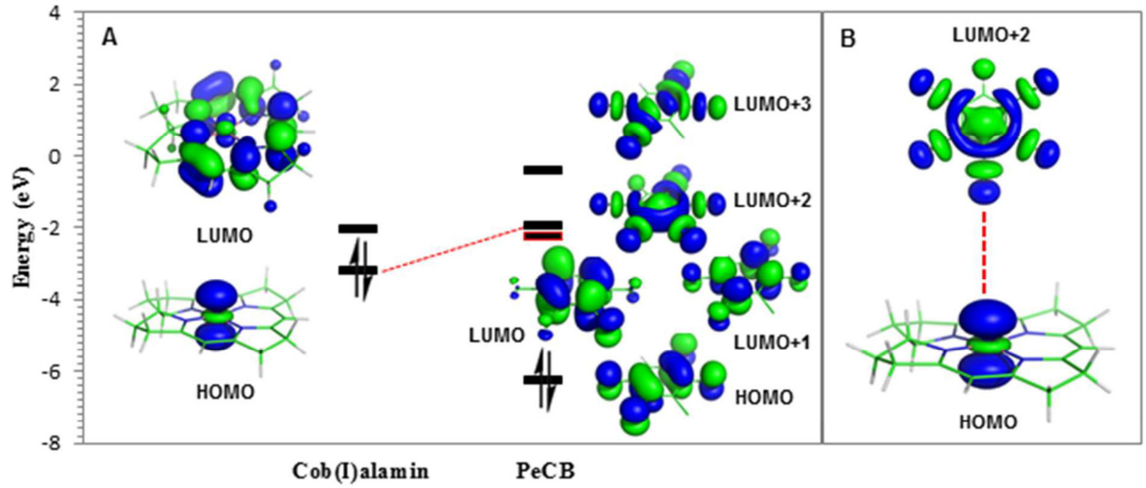

Figure 2. Molecular orbital interaction between cob(I)alamin and aromatic halides, taking pentachlorobenzene (PeCB) as example. A: HOMO and LUMO of cob(I)alamin (left) and HOMO as well as the lowest four unoccupied MOs (LUMO .. LUMO+3) of PeCB, with LUMO+2 as lowest σ* MO with a shape suitable for a favourable overlap with the Co(I) $3d_{z2}$ AO as almost only HOMO component. The orbital interaction is indicated through a red dashed line. The overlaid MO energy levels of LUMO and LUMO+1 have a red edging. B: Spatial cob(I)alamin-substrate interaction mode, illustrating the preferred electron-transfer interaction between Co(I) $3d_{z2}$ and $\sigma^*_{C\text{-}Cl}$ at aromatic carbon C_3 of the electron-accepting substrate PeCB (interaction connection in red). In A and B, the orbital amplitude values of 0.03 and –0.03 have been selected for visualizing the blue and green isosurfaces of the orbital lobes.

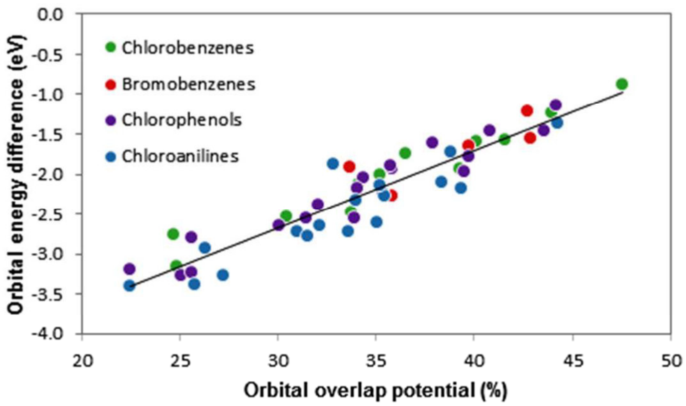

Figure 3. Orbital energy difference $\Delta\varepsilon_{DA} = \varepsilon_D - \varepsilon_A$ (cob(**I**)alamin HOMO – lowest substrate σ* MO) vs respective orbital overlap potential $c^2_{p,\text{ all X}}$ (eq. 6, section Material and Methods) covering the valence-shell *p* orbitals of all halogen substituents in a given substrate. For the 53 mono-ring aromatic halides (12 chlorobenzenes, 5 bromobenzenes, 19 chlorophenols, 17 chloroanilines), the linear regression equation $\Delta\varepsilon_{DA} = a \cdot c^2_{p,\text{ all X}} + b$ with $r^2 = 0.88$ has slope *a* = 0.096, intercept *b* = –5.6, and standard error = 0.22.

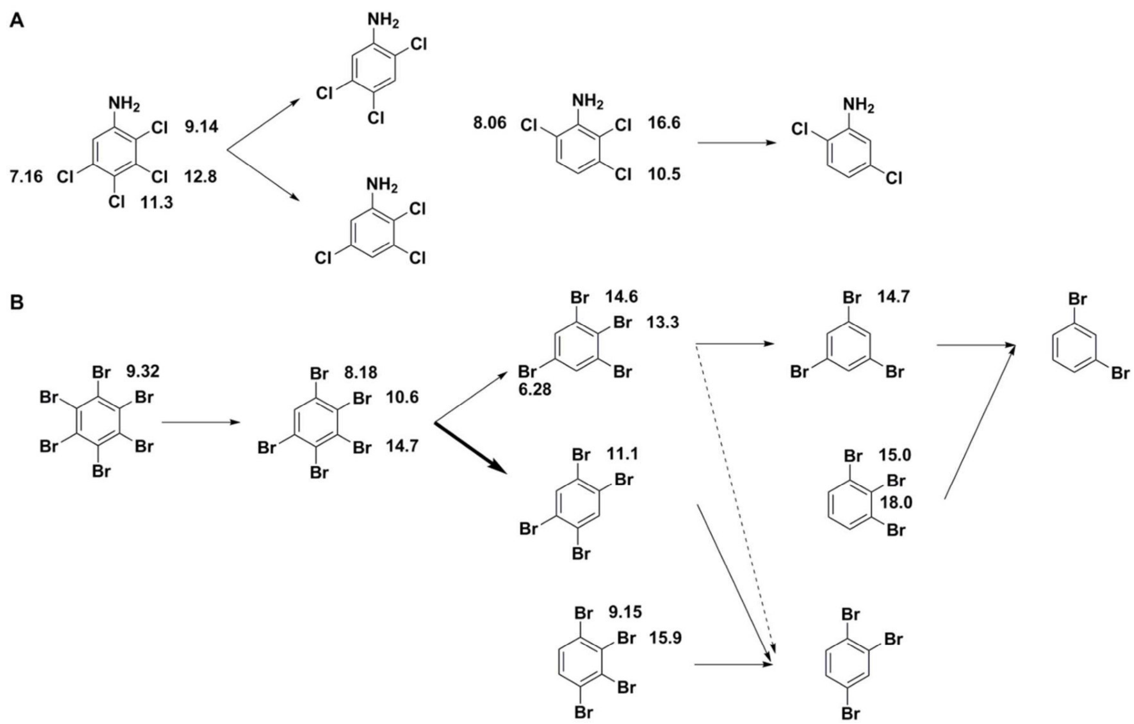

Figure 4. Predicted dehalogenation pathways of aryl halides for *Dehalococcoides mccartyi* strain CBDB1. A: Pathways for two commercially unavailable chloroanilines. B: Pathways for seven bromobenzenes whose dehalogenation has not yet been studied. The numerical values next to halogen atoms are the quantum chemically calculated c_{pX}^2 values (eq. 5, section Material and Methods) that represent the site-specific overlap potential of the halogen substituent through its valence-shell *p* orbitals of the lowest-energy σ* MO of the substrate. Bold arrows indicate major metabolites, and the dashed arrow shows a prediction different from experimental findings for the chlorobenzene counterpart.